

Supporting Information

The effects of near-surface atomic order on the catalytic properties of Cu₃Au and CuAu₃ intermetallics for the CO₂ reduction reaction

Lucas G. Verga^{1,2}, Yunzhe Wang², Tanmoy Chakraborty^{2,3}, Juarez L. F. Da Silva¹, and Tim Mueller²

¹ São Carlos Institute of Chemistry, University of São Paulo, PO Box 780, 13560-970, São Carlos, SP, Brazil.

² Department of Materials Science and Engineering, Johns Hopkins University, Baltimore, Maryland, 21218, United States.

³ Department of Chemistry, University of Warwick, Gibbet Hill Road, Coventry, CV4 7AL, United Kingdom.

E-mail: tmueller@jhu.edu

Contents

1. Computational Parameters	1
2. Reaction Free Energies	1
3. <i>K</i> -point convergence calculations	5
4. Cu, Au, Cu ₃ Au and CuAu ₃ Bulk Calculations	6
5. Calculations for Fitting CEs for Cu ₃ Au(100), CuAu ₃ (100), Cu ₃ Au(111), and CuAu ₃ (111) Slabs	7
6. Adsorption of CO ₂ Reduction Intermediates	9
6.1. COOH Adsorption	10
6.2. CO Adsorption.....	15
7. References	19

1. Computational Parameters

Table S1 shows the PAW projectors used in our calculations. The geometry optimizations and slab calculations were performed using a cutoff energy of 489 eV which is 12.5% higher than the highest ENMAX suggested among all PAW projectors.

Table S1: Technical details of the PAW projectors selected for the study. We show the recommended cutoff energy for each projector as well as the number of valence electrons.

Element	PAW Projector	ENMAX	Valency
Cu	Cu_GW 19May2006	417.039	11
Au	Au_GW 23Mar2010	248.344	11
C	C_GW_new 19Mar2012	413.992	4
O	O_GW 19Mar2012	434.431	6
H	H_GW 21Apr2008	300.000	1

Table S2 concatenates the values as convergence criteria for electronic self-consistent iterations, EDIFF, and ionic relaxation, EDIFFG used in our calculations with different purposes.

Table S2: Concatenation of technical details regarding convergence criteria for electronic self-consistent iterations, EDIFF, and ionic relaxation, EDIFFG.

Calculation type	EDIFF	EDIFFG
Bulk Stress Tensor	10^{-7} eV	-0.01 eV/ Å
Slab for CE fitting	10^{-4} eV	10-3 eV
Slabs for adsorption calculations	10^{-5} eV	-0.05 eV/ Å

2. Reaction free energies

The reaction diagrams are generated using the computational hydrogen electrode (CHE) model.^(1, 2) The CHE model treats proton-coupled electron (PCET) steps using the reversible hydrogen electrode (RHE) as a reference for the applied electrical potential (U). Thus, we assume that at U = 0 V vs RHE, the reaction ($1/2 \text{H}_2 \rightleftharpoons \text{H}^+ + \text{e}^-$) is in equilibrium for all pH and temperature values:

$$G^{H^+ + e^-} = \frac{1}{2} G^{H_2} - eU \quad (1)$$

This consideration makes the chemical potential for a proton-coupled electron equal to the chemical potential of gas-phase H_2 and allows for the applied potential to be adjusted for all PCETs. To obtain the free energies, we use:

$$G = E_{tot} + ZPE + \int C_p dT - TS + E_{sol} \quad (2)$$

where, E_{tot} is the total electronic energy, ZPE the zero-point energy, $\int C_p dT$ the enthalpic temperature, $-TS$ the entropy contributions, and E_{sol} the solvation correction.

The terms in $ZPE + \int C_p dT - TS$ were obtained using vibrational frequencies calculated via DFT as input values from the thermochemistry module from the atomic simulation environment package,(3) For adsorbed systems the quantities were obtained under the harmonic approximation for 298.15 K. We estimated solvation corrections using values for each adsorbate taken from the literature, where Peterson et al used an explicit hexagonal water overlayer and calculated solvation corrections as the stabilization generated by the presence of water (2) These values are listed in Table S3. As these values were nearly constant across Cu(100), Cu(111), Au(100), Au(111), we considered the sum $ZPE + \int C_p dT - TS + E_{sol}$ to be a correction, E_{cor} , that depends on the adsorbate but is independent of the substrate. The free energies can therefore be written as:

$$G = E_{tot} + E_{cor} \quad (3)$$

For non-adsorbed species, the quantities in $ZPE + \int C_p dT - TS$ were obtained in the ideal-gas limit in the thermochemistry module from the atomic simulation environment package, following the same approach and considering the same partial pressures detailed by Peterson et al.(2) All the values used for non-adsorbed species are summarized in Table S4. To account for the inconsistency of thermochemical data calculated with the PBE functional, we performed a series of calculations of gas-phase thermodynamic reactions containing CO₂ and CO and compared with experimental values. This approach is the same as the one performed in the literature to generate gas-phase corrections for such molecules.(2, 4) Table S4 shows the gas-phase correction (GPC) to the energy of CO and CO₂ of -0.35 and 0.10 eV, respectively.

Table S3: Calculated values of ZPE, $\int C_p dT$, and TS for *CO and *COOH adsorbed on Cu(100), Cu(111), Au(100), and Au(111) surfaces, together with the average value and standard deviation (std). The solvation energies, E_{sol} , were obtained from the work of Peterson et. al.(2).

*CO				
	ZPE (eV)	$\int C_p dT$ (eV)	TS (eV)	E_{sol} (eV)
Cu(100)	0.17	0.08	0.14	
Cu(111)	0.18	0.08	0.15	
Au(100)	0.19	0.07	0.12	
Au(111)	0.19	0.07	0.13	
Average	0.18	0.07	0.14	-0.10
std	0.01	0.00	0.01	
*COOH				
Cu(100)	0.61	0.10	0.21	
Cu(111)	0.60	0.11	0.21	
Au(100)	0.61	0.11	0.23	
Au(111)	0.61	0.11	0.24	
Average	0.61	0.11	0.22	-0.25
std	0.00	0.00	0.01	

Table S4: Calculated values of ZPEs, $\int C_p dT$, and TS for all gas-phase molecules, together with the gas-phase corrections and calculated adsorption energies, ΔE .

	ZPE (eV)	$\int C_p dT$ (eV)	TS (eV)	GPC (eV)	Esolv (eV)	Total (eV)	ΔE (eV)
CO2	0.31	0.10	0.66	0.11		-0.14	0.00
H2	0.27	0.09	0.43			-0.07	0.00
H2O	0.56	0.10	0.67			-0.01	0.00
CO [‡]	0.13	0.10	0.00	-0.35	-0.10	-0.22	0.76
CO(g)	0.13	0.10	0.67	-0.35		-0.79	0.76

Table S5: Reaction enthalpies (eV) calculated with our PBE+D3 approach compared with the experimental reference values from NIST.(5)

	ΔH_{Exp} (eV)	$\Delta H_{\text{PBE+D3}}$ (eV)	$(\Delta H_{\text{PBE+D3}} - \Delta H_{\text{Exp}})$
$\text{CO}_2 + 4\text{H}_2 \rightarrow \text{CH}_4 + 2\text{H}_2\text{O}$	-1.17	-1.08	0.09
$2\text{CO}_2 + 6\text{H}_2 \rightarrow \text{C}_2\text{H}_4 + 4\text{H}_2\text{O}$	-0.59	-0.29	0.30
$2\text{CO}_2 + 7\text{H}_2 \rightarrow \text{C}_2\text{H}_6 + 4\text{H}_2\text{O}$	-1.63	-1.43	0.20
$3\text{CO}_2 + 10\text{H}_2 \rightarrow \text{C}_3\text{H}_8 + 6\text{H}_2\text{O}$	-2.20	-1.88	0.32
CO ₂ Correction			0.11
$\text{CO} + 3\text{H}_2 \rightarrow \text{CH}_4 + \text{H}_2\text{O}$	-1.47	-1.84	-0.37
$2\text{CO} + 4\text{H}_2 \rightarrow \text{C}_2\text{H}_4 + 2\text{H}_2\text{O}$	-1.19	-1.82	-0.62
$2\text{CO} + 5\text{H}_2 \rightarrow \text{C}_2\text{H}_6 + 2\text{H}_2\text{O}$	-2.23	-2.96	-0.73
$3\text{CO} + 7\text{H}_2 \rightarrow \text{C}_3\text{H}_8 + 3\text{H}_2\text{O}$	-3.08	-4.17	-1.09
CO Correction			-0.35
$\text{CO}_2 + \text{H}_2 \rightarrow \text{CO} + \text{H}_2\text{O}$	0.30	0.76	0.46

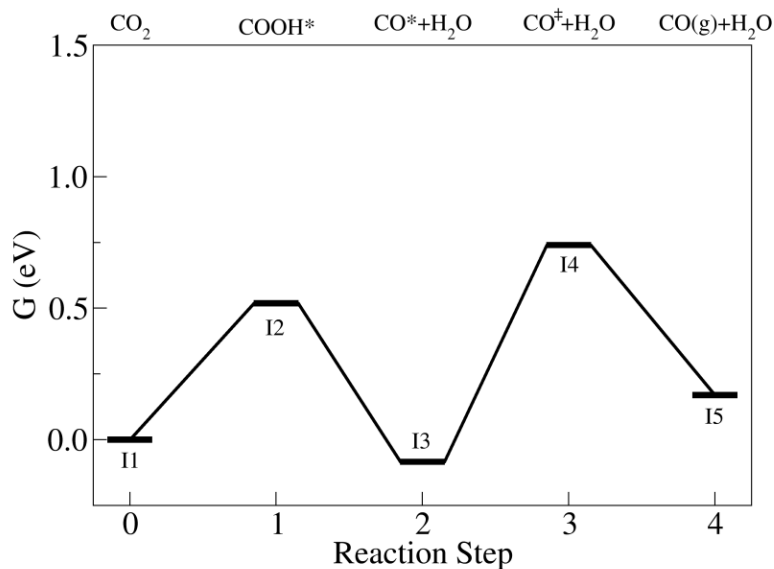


Figure S1: Illustration of a free energy diagram for CO₂ reduction considering hypothetical values for the mechanism $\text{CO}_2(\text{g}) \rightarrow * \text{COOH} \rightarrow * \text{CO} \rightarrow \text{CO}^\ddagger \rightarrow \text{CO}(\text{g})$.

As explained in the manuscript, we considered the following reaction mechanism for the CO₂RR to CO: $\text{CO}_2(\text{g}) \rightarrow * \text{COOH} \rightarrow * \text{CO} \rightarrow \text{CO}^\ddagger \rightarrow \text{CO}(\text{g})$. The change in free energy at each step along this pathway can be calculated as follows:

$$\begin{aligned}
\Delta G(I2-I1) &= (G^{*COOH} + G^{H^+e^-}) - (G^{CO_2} + 2G^{H^+e^-} + G^{slab}) \\
\Delta G(I3-I2) &= (G^{*CO} + G^{H_2O}) - (G^{*COOH} + G^{H^+e^-}) \\
\Delta G(I4-I3) &= (G^{CO^\ddagger} + G^{H_2O} + G^{slab}) - (G^{*CO} + G^{H_2O}) \\
\Delta G(I5-I4) &= (G^{CO(g)} + G^{H_2O} + G^{slab}) - (G^{CO^\ddagger} + G^{H_2O} + G^{slab})
\end{aligned} \tag{4}$$

Considering the determination of adsorption energies, ΔE , as described in the main manuscript, the determination of free energies as described in equation (1.3), and the E_{cor} calculated from the values from Table S3 and Table S4, we can rewrite the reaction energies for the reaction mechanism as:

$$\begin{aligned}
\Delta G(I2-I1) &= \Delta E^{*COOH} + (E_{cor}^{*COOH} - \Delta E^{CO_2} - E_{cor}^{CO_2} - 0.5E_{cor}^{H_2}) + eU = \Delta E^{*COOH} + 0.425 + eU \\
\Delta G(I3-I2) &= \Delta E^{*CO} - \Delta E^{*COOH} + (E_{cor}^{*CO} + E_{cor}^{H_2O} - E_{cor}^{*COOH} - 0.5E_{cor}^{H_2}) + eU = \Delta E^{*CO} - \Delta E^{*COOH} - 0.215 + eU \\
\Delta G(I4-I3) &= -\Delta E^{*CO} + (\Delta E^{CO^\ddagger} - E_{cor}^{*CO} + E_{cor}^{CO^\ddagger}) = -\Delta E^{*CO} + 0.53 \\
\Delta G(I5-I4) &= E_{cor}^{CO(g)} - E_{cor}^{CO^\ddagger} = -0.57
\end{aligned} \tag{5}$$

The state CO^\ddagger represents an activated state in which a CO molecule has desorbed from the surface. We calculated its free energy as the energy of a solvated CO molecule, where we include the same solvation correction as the one applied for CO and removed the entropic contributions.

3. K-point convergence calculations

To generate k -point grids for the DFT calculations, we employed efficient grids generated by the k -point grid server.^(6, 7) The density of these grids, as given by the minimum distance between points on the corresponding real space lattice (r_{min}), was determined using convergence tests (Figure S2). We found that for $r_{min} > 45 \text{ \AA}$, the formation energy of a copper slab is converged within 1 meV/atom, which is sufficient for this work.

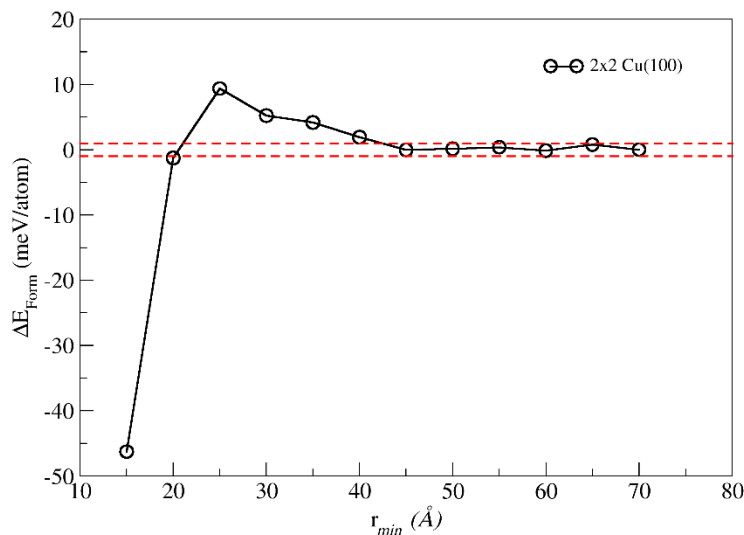


Figure S2: Relative formation energy, ΔE_{Form} , for different values of minimum distance between adjacent points in real space lattice, r_{min} , for a (2×2) Cu(100) surface with 7 layers. The dashed red lines indicate the 1 meV/atom limit as a reference.

4. Cu, Au, Cu₃Au and CuAu₃ Bulk Calculations

We determined the lattice parameters and analyzed the formation energies, E_{form} , for bulk Cu, Cu₃Au, CuAu, CuAu₃, and Au. Cu and Au were modeled using face-centered cubic (fcc) lattices, while the Cu-Au alloy were modeled based on ordered phases present at room temperature in the alloy phase diagram. Cu₃Au and CuAu₃ were modeled with L1₂ ordering, and CuAu was modeled with L1₀ ordering. The lattice parameters determined from DFT calculations for bulk Cu₃Au, CuAu, CuAu₃, shown in Figure S3 a) were used to generate the (100) and (111) slab models with the corresponding underlying bulk composition used for fitting the cluster expansion Hamiltonians, performing the Monte Carlo calculations, and studying adsorption. We show the values expected by Vegard's law only as a comparison between the calculated number and what one could expect from this approach.

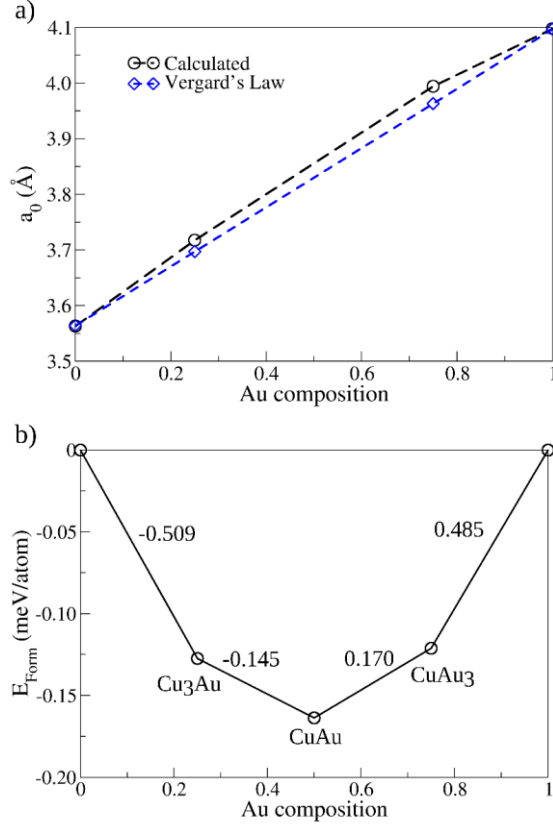


Figure S3: a) Lattice parameter and b) formation energies of bulk Cu, Cu_3Au , CuAu , CuAu_3 , and Au. The numbers in b) indicate the values used for the chemical potential window for Cu_3Au and CuAu_3 Monte Carlo calculations.

5. Calculations for Fitting CEs for $\text{Cu}_3\text{Au}(100)$, $\text{CuAu}_3(100)$, $\text{Cu}_3\text{Au}(111)$, and $\text{CuAu}_3(111)$ Slabs

The (3×3) and (4×4) slabs that were obtained from simulated annealing calculations during the fitting of the CE were relaxed with DFT and used to construct a convex hull of formation energies for each facet and underlying bulk composition (Figure S4, Figure S5). Structures were incrementally added to the training sets for the cluster expansions until no new structures appeared on the convex hull.

As discussed in the main manuscript the cluster expansions were fit using the Bayesian approach developed by Mueller et al.(8) Here, the inverse of the covariance matrix, Λ , for the prior distribution, was implemented with elements given by:

$$\lambda_{\alpha\alpha} = \begin{cases} 0 & \text{for } n_\alpha = 0 \\ \lambda_1 & \text{for } n_\alpha = 1 \\ e^{-\lambda_2} e^{\lambda_3 r_\alpha} n_\alpha^{\lambda_4} & \text{for } n_\alpha > 1 \end{cases} \quad (6)$$

$$\lambda_{\alpha\beta} = \begin{cases} 0 & \text{if } \alpha \text{ and } \beta \text{ are not congruent} \\ \lambda_5 \lambda_{\alpha\alpha} & \text{if } \alpha \text{ and } \beta \text{ are congruent} \end{cases}$$

where n_α and r_α are the number of sites and maximum distance between sites for a cluster function α , respectively. The regularization parameters λ_1 , λ_2 , λ_3 , λ_4 , and λ_5 were determined with a conjugate gradient algorithm applied to minimize the leave-one-out cross validation score. The parameters determine how the magnitudes of the ECIs are expected to change as a function of the number of sites in a cluster and the maximum distance between sites. For instance, λ_3 determines how rapidly the values of effective cluster interaction are expected to decay as a function of the maximum distance between clusters for a cluster function, while λ_4 shows to what extent we expect smaller contributions for cluster with a larger number of sites. The final values for the regularization parameters in the final CE were 3.72, 2.07, 0.83, 0.89 and 0.69 for Cu₃Au(100), 2.86, 0.66, 0.31, 1.96 and 2.35 for Cu₃Au(111), 9.98, 3.04, 1.09, 0.96 and 1.82 for CuAu₃(100), and 3.44, 0.80, 0.72, 1.52 and 0.73 for CuAu₃(111), where the units of distance are Angstroms, the units of energy are eV / primitive cell, and the units of the regularization parameters are set to ensure that the regularization term has units of energy squared, so that it can be added to the square error term.

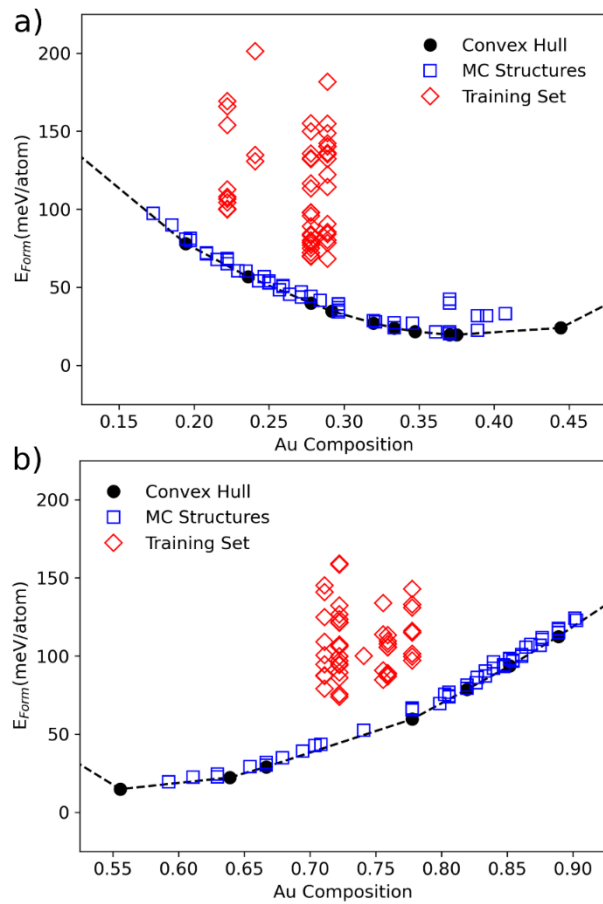


Figure S4: Formation energies calculated during the fitting of the CE Hamiltonian, together with the convex hull for a) $\text{Cu}_3\text{Au}(100)$ and b) $\text{CuAu}_3(100)$.

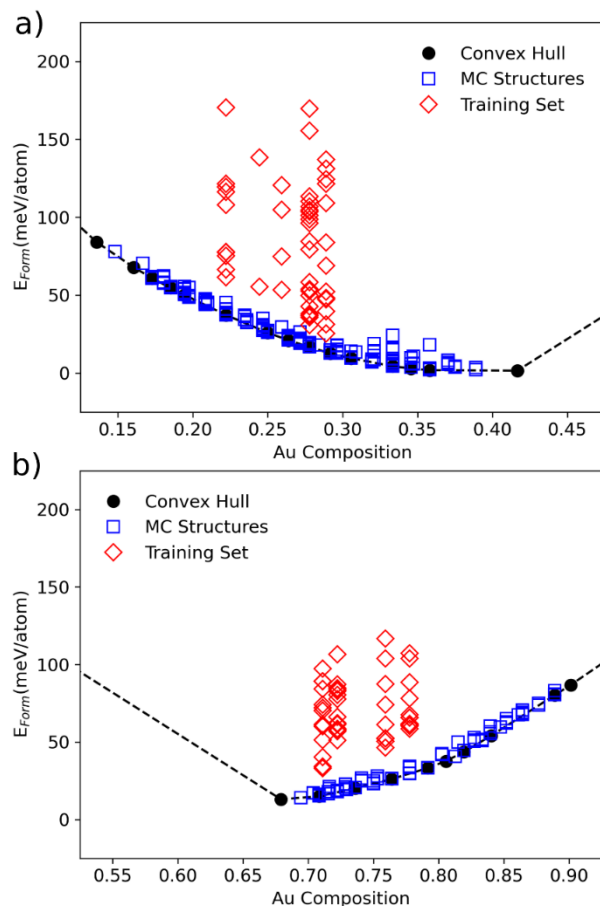


Figure S5: Formation energies calculated during the fitting of the CE Hamiltonian, together with the convex hull for a) $\text{Cu}_3\text{Au}(111)$ and b) $\text{CuAu}_3(111)$.

6. Adsorption of CO_2 Reduction Intermediates

Figures S6 to S15 illustrate the adsorbed COOH and CO configuration used to analyze the catalytic activity of the alloy surfaces in the main manuscript. We show results for all sites with a prevalence higher than 0.1% during the GCMC calculations for each facet and composition using only the nearest neighbors of each site in the representation vector used to distinguish them. After analyzing different molecule configurations near or at each site, we selected the most stable configuration, which are illustrated below, to represent each adsorption site on Figures S6 to S15. For the free energy diagrams in the manuscript, we only considered the sites found with our initial approach, i.e., adsorption sites found as distinct based on the atom closest to the molecule and its first-nearest neighbors.

We also analyzed our GCMC calculations using a vector to distinguish adsorption sites that included all the previous information of first neighbors and two additional features, namely, 1) the number of Cu second-nearest-neighbors, $N(\text{Cu}2\text{nd})$; 2) the average of the coordination number of all $N(\text{Cu}2\text{nd})$. This strategy was employed to consider variations in the second-neighbors chemical composition of the adsorption sites. For this strategy, we only calculated CO and COOH adsorption for the adsorption sites that presented i) a prevalence higher than 0.1% during the

GCMC calculations for each facet and composition and ii) the same nearest neighbors characteristics as the sites from the first round of selection that presented U_{onset} close to the best sites described in the main manuscript. Thus, we managed to investigate how changes in the second-nearest-neighbors of the best adsorption sites would affect the calculated adsorption energies and further analyze to what extent our original strategy was able to differentiate adsorption sites. From the result displayed in Figures S6 to S15 and Table S6 to Table S13, we see that the change in the second-nearest-neighbors generates changes in the ΔE of CO and COOH that were generally no more than 0.1 eV, with the only exception being Site 2 for $\text{Cu}_3\text{Au}(111)$ surfaces, for which the spreads in CO and COOH adsorption energies were 0.18 and 0.23 eV, respectively.

6.1. COOH Adsorption

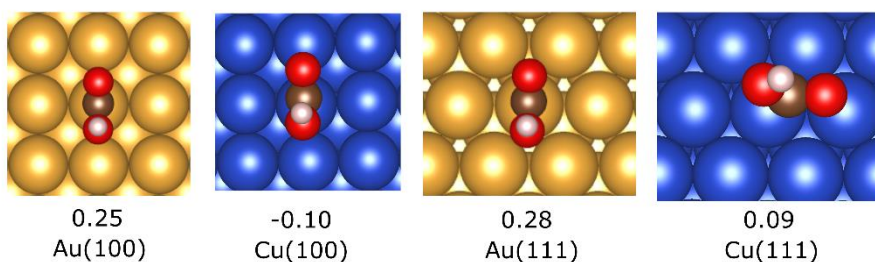


Figure S6: COOH adsorbed on monometallic surfaces with the calculated ΔE (eV).

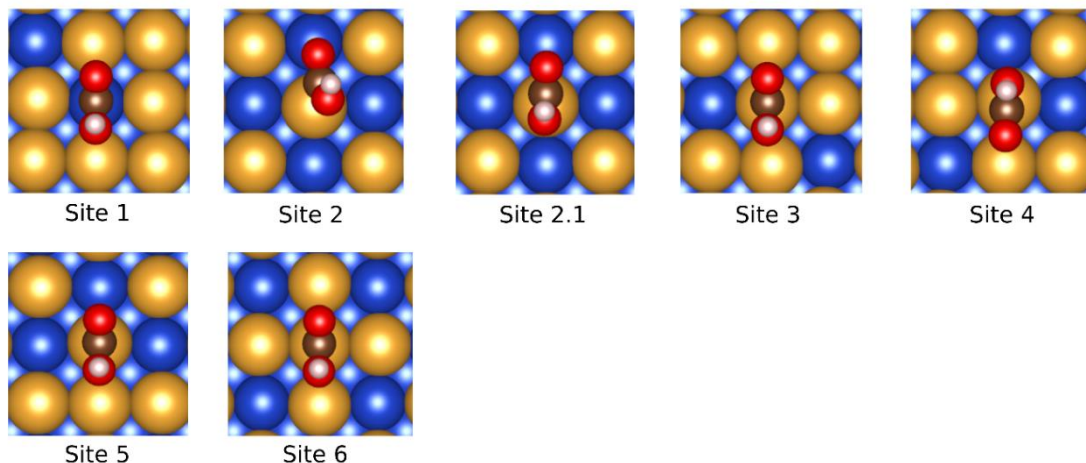


Figure S7: COOH adsorbed on different sites of $\text{Cu}_3\text{Au}(100)$ surfaces.

Table S6: COOH adsorbed on different sites of Cu₃Au(100) surfaces together with their adsorption energies, ΔE (eV), the original representation vector containing information about the top site nearest to the adsorbate and its first neighbors, and the representation vector containing additional information about the second neighbors. We mark in bold the sites from our original representation that were used to test the impact of second nearest neighbors.

System	ΔE (eV)	Original Representation Vector	Representation Vector with 2 nd Nearest Neighbors
Site 1	0.52	(1, 4, 12.00)	(1, 4, 12.00, 2, 10.00)
Site 2	0.16	(0, 8, 10.00)	(0, 8, 10.00, 1, 12.00)
Site 2.1	0.23	(0, 8, 10.00)	(0, 8, 10.00, 0, 0.00)
Site 3	0.32	(0, 5, 11.20)	(0, 5, 11.20, 1, 8.00)
Site 4	0.32	(0, 6, 10.66)	(0, 6, 10.66, 1, 8.00)
Site 5	0.30	(0, 7, 10.28)	(0, 7, 10.28, 1, 12.00)
Site 6	0.30	(0, 4, 12.00)	(0, 4, 12.00, 4, 8.00)

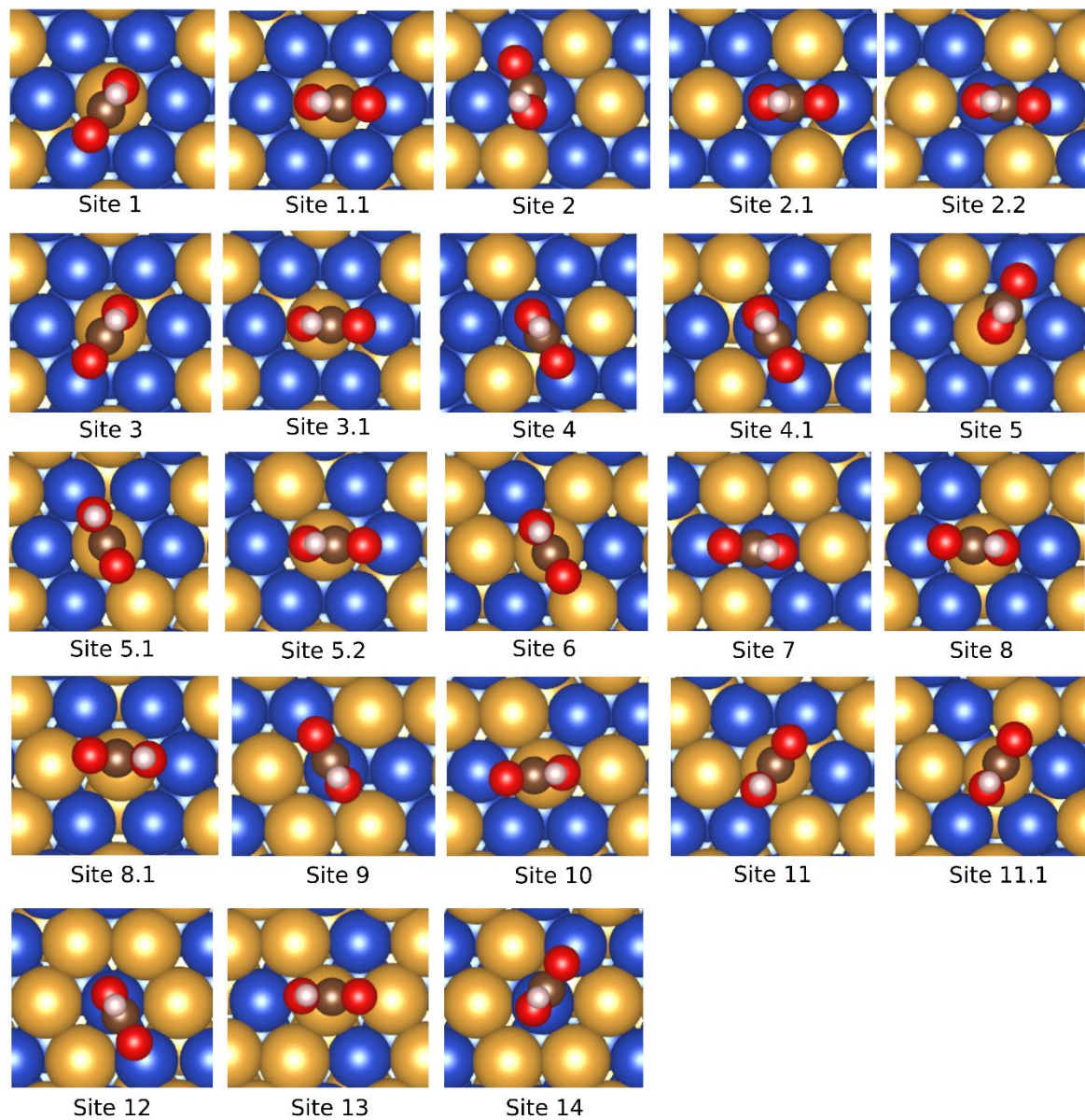


Figure S8: COOH adsorbed on different sites of Cu₃Au(111) surfaces.

Table S7: COOH adsorbed on different sites of Cu₃Au(111) surfaces together with their adsorption energies, ΔE (eV), the original representation vector containing information about the top site nearest to the adsorbate and its first neighbors, and the representation vector containing additional information about the second neighbors. We mark in bold the sites from our original representation that were used to test the impact of second nearest neighbors.

System	ΔE (eV)	Original Representation Vector	Representation Vector with 2 nd Nearest Neighbors
Site 1	0.25	(0, 9, 10.00)	(0, 9, 10.00, 2,12.00)
Site 1.1	0.33	(0, 9, 10.00)	(0, 9, 10.00, 3,12.00)
Site 2	0.19	(1, 6, 10.50)	(1, 6, 10.50, 3,12.00)
Site 2.1	0.27	(1, 6, 10.50)	(1, 6, 10.50, 2,12.00)
Site 2.2	0.42	(1, 6, 10.50)	(1, 6, 10.50, 1,12.00)
Site 3	0.13	(0, 8, 9.75)	(0, 8, 9.75, 3,12.00)
Site 3.1	0.13	(0, 8, 9.75)	(0, 8, 9.75, 2,12.00)
Site 4	0.23	(1, 5, 10.20)	(1, 5, 10.20, 3,12.00)
Site 4.1	0.33	(1, 5, 10.20)	(1, 5, 10.20, 2,12.00)
Site 5	0.25	(0, 8, 10.12)	(0, 8, 10.12, 3,12.00)
Site 5.1	0.27	(0, 8, 10.12)	(0, 8, 10.12, 2,12.00)
Site 5.2	0.30	(0, 8, 10.12)	(0, 8, 10.12, 1,12.00)
Site 6	0.37	(0, 6, 10.50)	(0, 6, 10.50, 1,12.00)
Site 7	0.42	(1, 5, 10.80)	(1, 5, 10.80, 3,12.00)
Site 8	0.20	(0, 7, 9.86)	(0, 7, 9.86, 3,12.00)
Site 8.1	0.16	(0, 7, 9.86)	(0, 7, 9.86, 2,12.00)
Site 9	0.39	(1, 4, 10.50)	(1, 4, 10.50, 3,12.00)
Site 10	0.34	(0, 7, 10.28)	(0, 7, 10.28, 2,12.00)
Site 11	0.25	(0, 6, 10.00)	(0, 6, 10.00, 3,12.00)
Site 11.1	0.20	(0, 6, 10.00)	(0, 6, 10.00, 2,12.00)
Site 12	0.51	(1, 4, 11.25)	(1, 4, 11.25, 2,12.00)
Site 13	0.31	(0, 5, 10.20)	(0, 5, 10.20, 2,12.00)
Site 14	0.45	(1, 3, 11.00)	(1, 3, 11.00, 3,12.00)

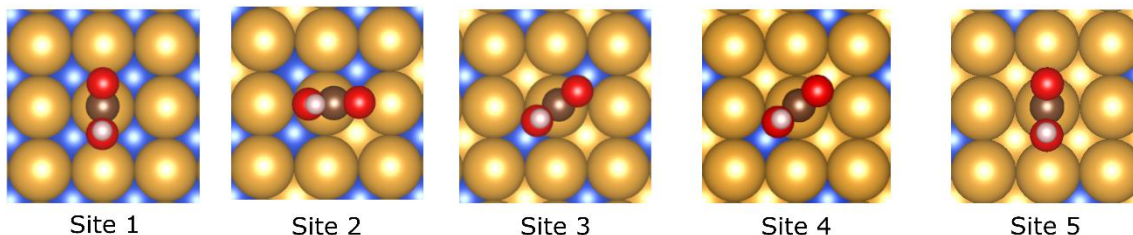


Figure S9: COOH adsorbed on different sites of $\text{CuAu}_3(100)$ surfaces.

Table S8: COOH adsorbed on different sites of $\text{CuAu}_3(100)$ surfaces together with their adsorption energies, ΔE (eV), the original representation vector containing information about the top site nearest to the adsorbate and its first neighbors, and the representation vector containing additional information about the second neighbors.

System	ΔE (eV)	Original Representation Vector	Representation Vector with 2 nd Nearest Neighbors
Site 1	0.46	(0, 4, 12.00)	(0, 4, 12.00, 0, 0.00)
Site 2	0.28	(0, 3, 12.00)	(0, 3, 12.00, 0, 0.00)
Site 3	0.21	(0, 2, 12.00)	(0, 2, 12.00, 0, 0.00)
Site 4	0.22	(0, 1, 12.00)	(0, 1, 12.00, 0, 0.00)
Site 5	0.21	(0, 0, 0.00)	(0, 0, 0.00, 0, 0.00)

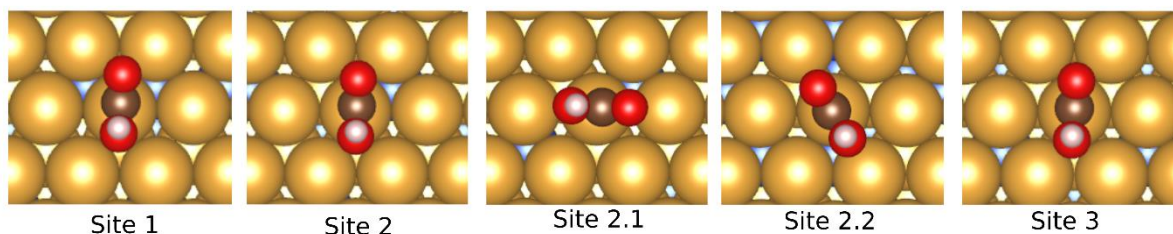


Figure S10: COOH adsorbed on different sites of $\text{CuAu}_3(111)$ surfaces.

Table S9 : COOH adsorbed on different sites of $\text{CuAu}_3(111)$ surfaces together with their adsorption energies, ΔE (eV), the original representation vector containing information about the top site nearest to the adsorbate and its first neighbors, and the representation vector containing additional information about the second neighbors. We mark in bold the sites from our original representation that were used to test the impact of second nearest neighbors.

System	ΔE (eV)	Original Representation Vector	Representation Vector with 2 nd Nearest Neighbors
Site 1	0.33	(0, 2, 12.00)	(0, 2, 12.00, 0, 0.00)
Site 2	0.29	(0, 1, 12.00)	(0, 1, 12.00, 0, 0.00)
Site 2.1	0.36	(0, 1, 12.00)	(0, 1, 12.00, 1, 12.00)
Site 2.2	0.31	(0, 1, 12.00)	(0, 1, 12.00, 2, 12.00)
Site 3	0.34	(0, 0, 0.00)	(0, 0, 0.00, 2, 12.00)

6.2.CO Adsorption

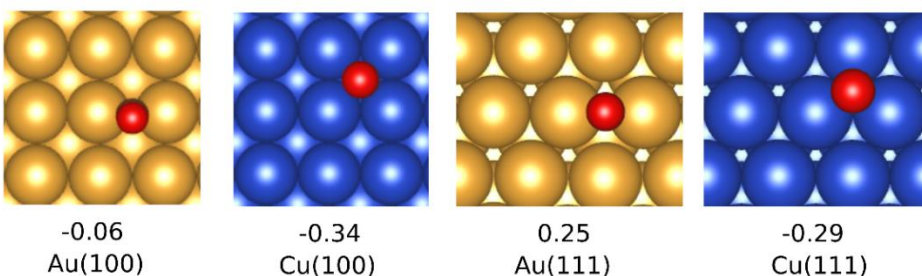


Figure S11: CO adsorbed on monometallic surfaces with the calculated ΔE (eV).

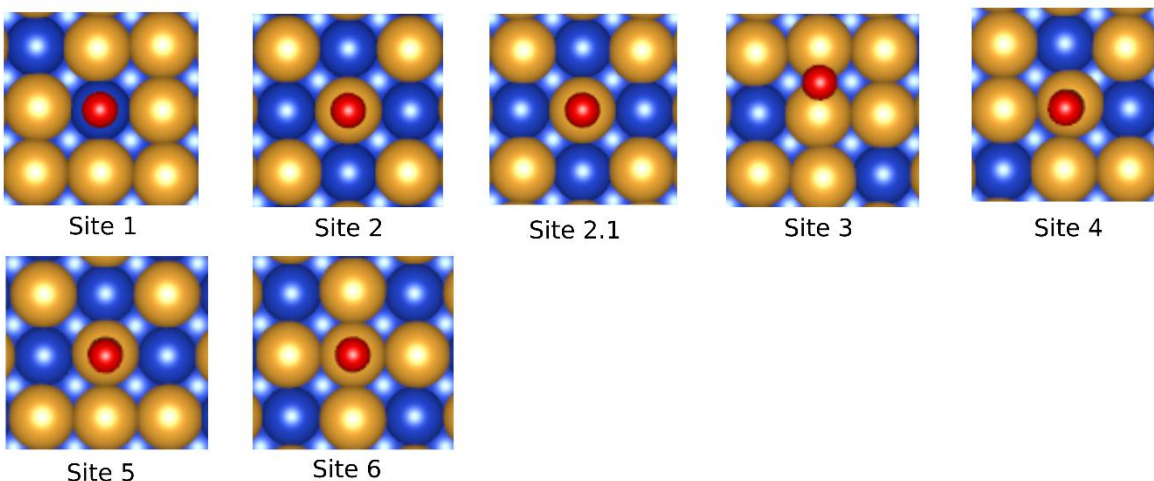


Figure S12: CO adsorbed on different sites of $\text{Cu}_3\text{Au}(100)$ surfaces.

Table S10: CO adsorbed on different sites of $\text{Cu}_3\text{Au}(100)$ surfaces together with their adsorption energies, ΔE (eV), the original representation vector containing information about the top site nearest to the adsorbate and its first neighbors, and the representation vector containing additional information about the second neighbors. We mark in bold the sites from our original representation that were used to test the impact of second nearest neighbors.

System	ΔE (eV)	Original Representation Vector	Representation Vector with 2 nd Nearest Neighbors
Site 1	0.05	(1, 4, 12.00)	(1, 4, 12.00, 2, 10.00)
Site 2	0.15	(0, 8, 10.00)	(0, 8, 10.00, 1, 12.00)
Site 2.1	0.10	(0, 8, 10.00)	(0, 8, 10.00, 0, 0.00)
Site 3	0.24	(0, 5, 11.20)	(0, 5, 11.20, 1, 8.00)
Site 4	0.19	(0, 6, 10.66)	(0, 6, 10.66, 1, 8.00)
Site 5	0.20	(0, 7, 10.28)	(0, 7, 10.28, 1, 12.00)
Site 6	0.26	(0, 4, 12.00)	(0, 4, 12.00, 4, 8.00)

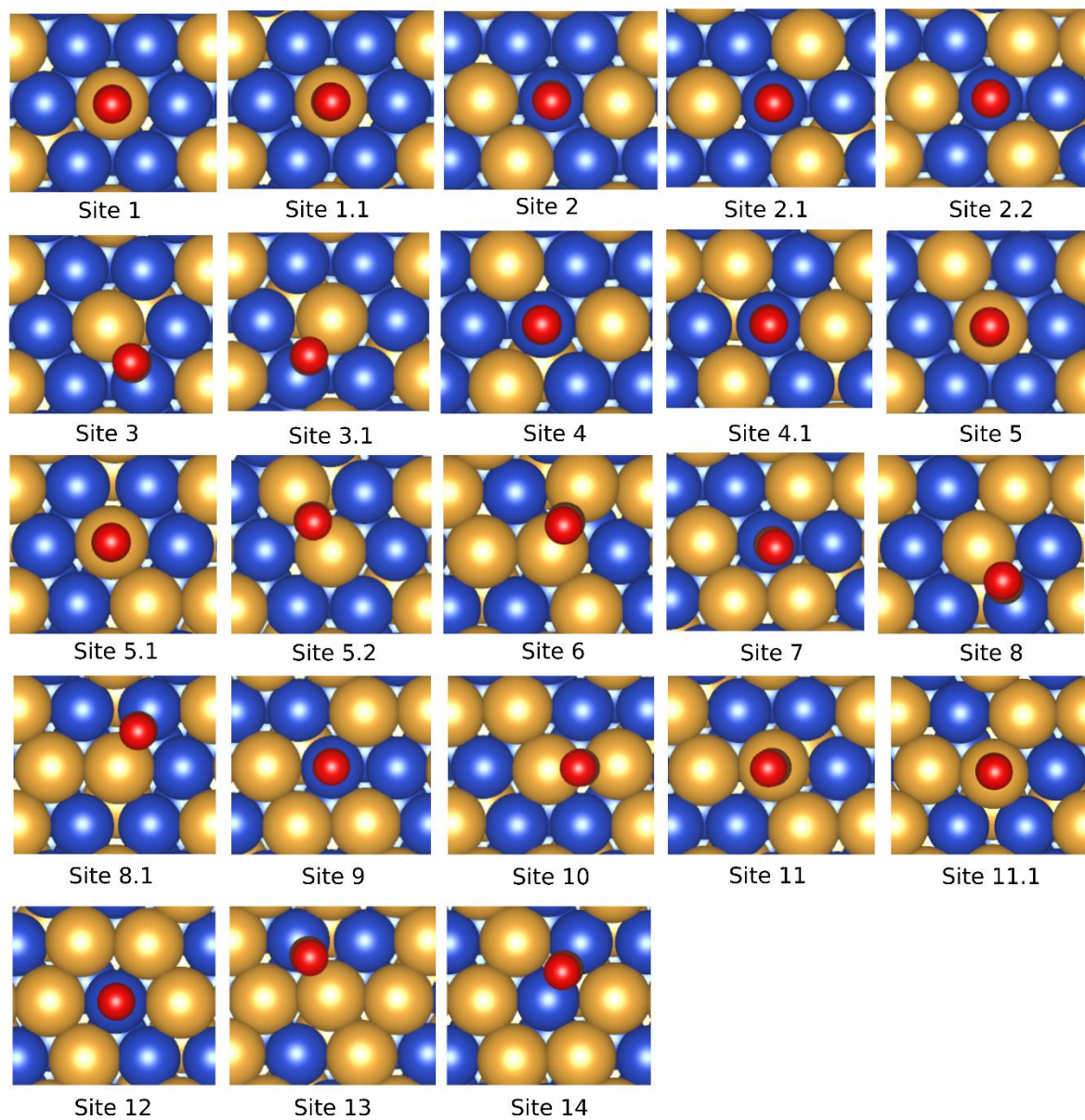


Figure S13: CO adsorbed on different sites of Cu₃Au(111) surfaces.

Table S11: CO adsorbed on different sites of Cu₃Au(111) surfaces together with their adsorption energies, ΔE (eV), \mathbf{t} the original representation vector containing information about the top site nearest to the adsorbate and its first neighbors, and the representation vector containing additional information about the second neighbors. We mark in bold the sites from our original representation that were used to test the impact of second nearest neighbors.

System	ΔE (eV)	Original Representation Vector	Representation Vector with 2 nd Nearest Neighbors
Site 1	0.25	(0, 9, 10.00)	(0, 9, 10.00, 2,12.00)
Site 1.1	0.28	(0, 9, 10.00)	(0, 9, 10.00, 3,12.00)
Site 2	-0.12	(1, 6, 10.50)	(1, 6, 10.50, 3,12.00)
Site 2.1	-0.10	(1, 6, 10.50)	(1, 6, 10.50, 2,12.00)
Site 2.2	0.06	(1, 6, 10.50)	(1, 6, 10.50, 1,12.00)
Site 3	0.02	(0, 8, 9.75)	(0, 8, 9.75, 3,12.00)
Site 3.1	0.06	(0, 8, 9.75)	(0, 8, 9.75, 2,12.00)
Site 4	-0.09	(1, 5, 10.20)	(1, 5, 10.20, 3,12.00)
Site 4.1	-0.05	(1, 5, 10.20)	(1, 5, 10.20, 2,12.00)
Site 5	0.29	(0, 8, 10.12)	(0, 8, 10.12, 3,12.00)
Site 5.1	0.28	(0, 8, 10.12)	(0, 8, 10.12, 2,12.00)
Site 5.2	0.30	(0, 8, 10.12)	(0, 8, 10.12, 1,12.00)
Site 6	0.31	(0, 6, 10.50)	(0, 6, 10.50, 1,12.00)
Site 7	0.05	(1, 5, 10.80)	(1, 5, 10.80, 3,12.00)
Site 8	0.02	(0, 7, 9.86)	(0, 7, 9.86, 3,12.00)
Site 8.1	0.02	(0, 7, 9.86)	(0, 7, 9.86, 2,12.00)
Site 9	0.01	(1, 4, 10.50)	(1, 4, 10.50, 3,12.00)
Site 10	0.36	(0, 7, 10.28)	(0, 7, 10.28, 2,12.00)
Site 11	0.30	(0, 6, 10.00)	(0, 6, 10.00, 3,12.00)
Site 11.1	0.25	(0, 6, 10.00)	(0, 6, 10.00, 2,12.00)
Site 12	0.12	(1, 4, 11.25)	(1, 4, 11.25, 2,12.00)
Site 13	0.13	(0, 5, 10.20)	(0, 5, 10.20, 2,12.00)
Site 14	0.10	(1, 3, 11.00)	(1, 3, 11.00, 3,12.00)

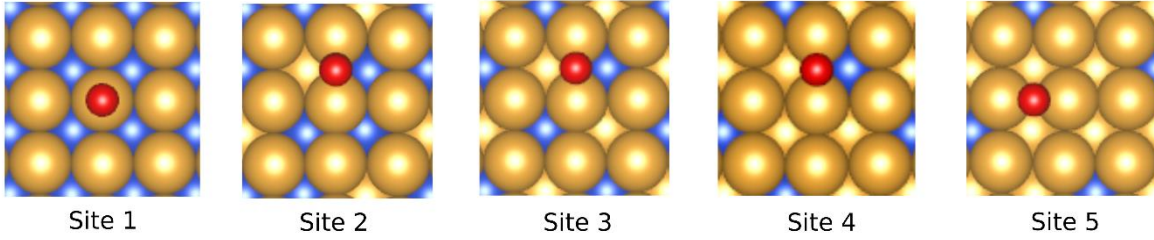


Figure S14: CO adsorbed on different sites of $\text{CuAu}_3(100)$ surfaces.

Table S12: CO adsorbed on different sites of $\text{CuAu}_3(100)$ surfaces together with their adsorption energies, ΔE (eV), the original representation vector containing information about the top site nearest to the adsorbate and its first neighbors, and the representation vector containing additional information about the second neighbors.

System	ΔE (eV)	Original Representation Vector	Representation Vector with 2 nd Nearest Neighbors
Site 1	0.20	(0, 4, 12.00)	(0, 4, 12.00, 0, 0.00)
Site 2	0.10	(0, 3, 12.00)	(0, 3, 12.00, 0, 0.00)
Site 3	0.06	(0, 2, 12.00)	(0, 2, 12.00, 0, 0.00)
Site 4	0.02	(0, 1, 12.00)	(0, 1, 12.00, 0, 0.00)
Site 5	0.04	(0, 0, 0.00)	(0, 0, 0.00, 0, 0.00)

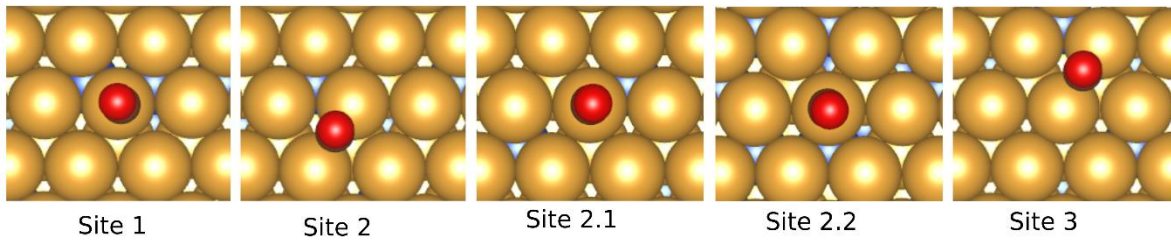


Figure S15: CO adsorbed on different sites of $\text{CuAu}_3(111)$ surfaces.

Table S13: CO adsorbed on different sites of $\text{CuAu}_3(111)$ surfaces together with their adsorption energies, ΔE (eV), the original representation vector containing information about the top site nearest to the adsorbate and its first neighbors, and the representation vector containing additional information about the second neighbors. We mark in bold the sites from our original representation that were used to test the impact of second nearest neighbors.

System	ΔE (eV)	Original Representation Vector	Representation Vector with 2 nd Nearest Neighbors
Site 1	0.33	(0, 2, 12.00)	(0, 2, 12.00, 0, 0.00)
Site 2	0.31	(0, 1, 12.00)	(0, 1, 12.00, 0, 0.00)
Site 2.1	0.33	(0, 1, 12.00)	(0, 1, 12.00, 1, 12.00)
Site 2.2	0.32	(0, 1, 12.00)	(0, 1, 12.00, 2, 12.00)

Site 3	0.31	(0, 0, 0.00)	(0, 0, 0.00, 2, 12.00)
--------	------	--------------	------------------------

7. References

1. J. R. Kitchin, J. K. Nørskov, M. A. Barteau, J. G. Chen, Role of Strain and Ligand Effects in the Modification of the Electronic and Chemical Properties of Bimetallic Surfaces. *Physical Review Letters* **93**, 156801 (2004).
2. A. A. Peterson, F. Abild-Pedersen, F. Studt, J. Rossmeisl, J. K. Nørskov, How Copper Catalyzes the Electroreduction of Carbon Dioxide into Hydrocarbon Fuels. *Energy & Environmental Science* **3**, 1311-1315 (2010).
3. A. Hjorth Larsen *et al.*, The Atomic Simulation Environment—A Python Library for Working with Atoms. *Journal of Physics: Condensed Matter* **29**, 273002 (2017).
4. L. Cao *et al.*, Mechanistic Insights for Low-Overpotential Electroreduction of CO₂ to CO on Copper Nanowires. *ACS Catalysis* **7**, 8578-8587 (2017).
5. P. J. Linstrom, W. G. Mallard. (Journal of Chemical and Engineering Data, 2001), vol. 20899.
6. Y. Wang, P. Wisesa, A. Balasubramanian, S. Dwaraknath, T. Mueller, Rapid Generation of Optimal Generalized Monkhorst-Pack Grids. *Computational Materials Science* **187**, 110100 (2021).
7. P. Wisesa, K. A. McGill, T. Mueller, Efficient generation of generalized Monkhorst-Pack grids through the use of informatics. *Physical Review B* **93**, 155109 (2016).
8. T. Mueller, G. Ceder, Bayesian Approach to Cluster Expansions. *Physical Review B* **80**, 024103 (2009).